Use of peaks and troughs in the horizontal-to-vertical spectral ratio of ambient noise for Rayleigh-wave dispersion curve picking

by

José Piña-Flores, [1-2] Martín Cárdenas-Soto, [1] Antonio García-Jerez,[3] Helena Seivane,[3] Francisco Luzón,[3] and Francisco J. Sánchez-Sesma[4]

(1) Facultad de Ingeniería, Universidad Nacional Autónoma de México; CU, Circuito Escolar; Coyoacán 04510; CDMX, México. Email: jpf@unam.mx and martinc@unam.mx
(2) Posgrado de Ingeniería, Universidad Nacional Autónoma de México; Edificio "S" "Bernardo Quintana Arrioja", Primer Piso, Facultad de Ingeniería, Cd. Universitaria, CDMX. C.P. 04510.
(3) Departamento de Química y Física, Universidad de Almería. 04120 Almería, Spain. Email: agarcia-jerez@ual.es, hsr084@ual.es and fluzon@ual.es
(4) Instituto de Ingeniería, Universidad Nacional Autónoma de México, C.U., Coyoacán 04510 D.F., México. E-mail: sesma@unam.mx

Abstract

To assist in the identification of fundamental-mode dispersion curves of Rayleigh waves in dispersion diagrams, we explore the relation between the shape of the horizontal-to-vertical spectral-ratio (HVSR) of ambient seismic noise and the shape of the dispersion curves for phase and group velocities in a stratified medium. We propose to use the information coming from the HVSR to identify the osculation zones and multi-mode effects and to locate inflection points and critical points in the observed phase and group dispersion diagrams of Rayleigh waves. The relationship between these curves has been numerically investigated for some models consisting of one and two homogeneous layers overlying a half-space, with velocities increasing downwards. It is primarily found that the first minimum in the HVSR appears close to the frequency of the inflection point of the fundamental mode of phase velocity. In addition, the osculation and multimode effects occur between frequencies of the fundamental peak and the first minimum of the HVSR. On the other hand,

the frequencies of the minima in HVSR closely approximate the critical points of the fundamental-mode group-velocity dispersion curve, even better than the inflection points of the fundamental-mode phase-velocity curve. Finally, we show an example of experimental identification of fundamental-mode phase and group dispersion curves supported by the shape of the HVSR, obtaining a reliable velocity profile through the simultaneous inversion of these three curves.

1. Introduction

In the last two decades, the ambient seismic noise (ASN) has been extensively used to obtain Rayleigh wave dispersion diagrams. The primary objective of these studies is to obtain S-wave velocity profiles and to evaluate site effects (see Xia *et al*., 1999; Bonnefoy-Claudet *et al*., 2006; Foti *et al*., 2011). Different geophysical methods are allowing the retrieval of dispersion curves using ASN signals, among which the most important are the following: 1.- Spatial Autocorrelation (SPAC, Aki, 1957; Köhler *et al*., 2007; García-Jerez *et al*., 2008); 2.- frequency-wavenumber analysis (FK, Capon, 1969; Ohori *et al*., 2002); 3.- passive Multichannel Analysis of Surface Waves (MASW, Dai *et al.,* 2019, Coelho *et al*., 2018, Mi *et al.,* 2017); 4.- Refraction Microtremor (ReMi, Louie, 2001).

Dispersion curves picking in frequency-velocity or equivalent diagrams is generally made manually, identifying high energy bands with segments of dispersion curves of a particular mode. Thus, interpretation errors can be made with some probability. In methods such as the SPAC or with limited array setups, only an effective phase velocity dispersion curve can be usually picked, probably as a combination of several Rayleigh wave modes (Tokimatsu *et al*., 1992; Zhang, 2011). The transition between different modes can even contain leaky waves which cannot be interpreted in terms of normal Rayleigh-wave modes (Gao *et al*., 2014; García-Jerez & Sánchez-Sesma, 2015). When the propagation medium has a high impedance contrast or low velocity zones (Mi *et al*., 2018), the effective phase-velocity dispersion curve of Rayleigh and Love waves often shows jumps due to mode osculation effects and/or significant contributions of higher modes (Tokimatsu *et al*., 1992; Ikeda *et al*., 2012; Pan *et al.,* 2013; Gao *et al*., 2016). This multi-mode effects can even be due to the directional contribution of noise sources (Ma *et al*., 2016) or to the presence of surface topography which can strongly influence the energy distribution in a dispersion image at high frequency (Zeng *et al*., 2012; Ning *et al*., 2018).

When working with a limited number of stations, the lack of resolution in the dispersion diagram can make it difficult to separate the different modes (e.g. Lin *et al.*, 2017), mainly when there are osculation effects. Incorrect identification of the modes will usually lead to an overestimation of S-wave velocities and errors in depths during the inversion (Zhang & Chang, 2009; Gao *et al.*, 2016). Separation of higher-mode dispersion curves from the fundamental-mode group velocity gets even more complicated due to the existence of crossings between different modes at different frequencies (see e.g. Baena-Rivera *et al.*, 2016). However, when a correct identification of fundamental mode and higher modes is made, for phase and group velocities, the incorporation of higher modes in an inversion process allows to get better information about the velocity profile, increasing the depth of investigation and the resolution of the model (Maraschini *et al.*, 2010).

Different studies have tried to mitigate the problem of mode identification. Tokimatsu *et al.* (1992) discussed the effects of multiple modes on Rayleigh wave dispersion curves to reduce the non-uniqueness of shear wave velocity profiles, proposing the definition of effective dispersion curves that appear as a combination of modal curves. Lunedei & Albarello (2009) found an expression for the effective dispersion curves as a function of the modal phase-velocity dispersion curves. This equation has been used by Farrugia *et al.* (2016) to obtain velocity profiles with effective dispersion curves. Moreover, Lai *et al.* (2014) and Astaneh & Guddati (2016) presented explicit mathematical derivations for different definitions of the effective phase velocity of Rayleigh waves in an isotropic elastic horizontally layered medium, based on analytical derivatives. These formulae can lead to the development of a new class of inversion algorithms capable of considering the influence of all modes of Rayleigh wave propagation.

Amplitude ratios, subsoil conditions and analysis of particle motion can help in modal separation. Boaga *et al.* (2013) examined the subsoil conditions and the common field acquisition procedures that can generate osculation effects in the Rayleigh wave dispersion curves. These osculation effects are linked to the Rayleigh wave ellipticity. These authors show *a priori* markers of subsoil conditions that can act as warnings against the osculation effects and relate these signs with those frequencies at which dispersion curves can be misidentified. Rivet *et al.* (2015) proposed to use the horizontal-to-vertical spectral-ratio (HVSR) from records of ASN for the identification of higher modes. They

3

independently inverted the dispersion curves assuming that they corresponded to (1) the fundamental mode and (2) the first higher mode. Afterward, they computed the theoretical HVSR for the obtained models and compared them with the observed HVSR, allowing the identification of the excitation mode.

In contrast, Ma *et al*. (2016) used the approach proposed by Tokimatsu *et al*. (1992) to distinguish the fundamental-mode excitation from the higher modes, observing the particle motion for Rayleigh waves in a period range of 1-10 sec. Besides, these authors found that the cut-off frequency of the first higher mode is controlled by the depth of the basement and coincides with the rapid decrement of the HVSR of the fundamental mode (ellipticity). Maranò *et al*. (2017) have succeeded in recovering the ellipticity of Rayleigh waves from records of ASN. They indicated that the phase angle of the ellipticity can be valuable information for mode separation. The ellipticity angle allows to accurately find the frequency of its singularities, which in turn correspond to a change in the direction of the particle motion from retrograde to retrograde or *vice versa*. Boué *et al*. (2016) also analyzed the particle motion in cross-correlations (CC) between pairs of stations to distinguish between fundamental- and higher-mode dispersion curves considering these differences in the motion direction.

More recently, Mi *et al.* (2019) proposed the separation of higher and fundamental modes of Rayleigh waves in the frequency - phase velocity (*f-v*) domain through the high-resolution linear Radon transformation. They also calculated the HVSR of Rayleigh waves for the fundamental mode from active seismic records. Finally, Maraschini *et al*. (2010) proposed a method to invert Rayleigh wave data in which the misfit function is a norm of the Thomson-Haskell matrix determinant evaluated at experimental dispersion data. The main advantage is the possibility of considering several modes simultaneously, without specifying to which mode each velocity belongs.

On the other hand, the HVSR is the simplest and the prevalent method to obtain the dominant frequency of the site by processing ASN recorded by a single station (e.g. Nakamura, 1989; Lermo & Chávez-García, 1993). Theoretical efforts have been carried out to find out the connection between this observable and the vertical distribution of elastic properties (e.g. Arai & Tokimatsu, 2004; Kawase *et al*., 2011). Modelling ASN as a diffuse field has shown excellent results (e.g. Sánchez-

4

Sesma *et al*., 2011; Spica *et al*., 2015; Lontsi *et al*., 2015). Actually, joint inversion of the HVSR and the fundamental and/or higher modes dispersion curves is a powerful and relatively simple scheme that mitigates trade-off issues between model parameters (e.g. Piña-Flores *et al*., 2017; Sivaram *et al*., 2018; García-Jerez *et al*., 2019).

In this work, we first explore the relationships between the dispersion curves of Rayleigh waves and the HVSR calculated under the diffuse field approach (DFA). Using two simple models with varying parameters, we show that the shape of the observed HVSR allows us to identify the dispersion curves of fundamental-mode Rayleigh waves preventing the contamination by higher modes. An application to array measurements performed at the Andarax river delta (Almeria, Spain) is presented. ASN data recorded by pentagonal arrays were analyzed by using the SPAC, FK and the cross-correlations between pairs of receivers. We took advantage of the characteristics of the HVSR to pick reliable phase and group dispersion curves of fundamental-mode Rayleigh waves. A joint inversion of these curves under the DFA led to an improved velocity profile for this site. Finally, forward computations show that some of the information in the SPAC, FK and CC dispersion diagrams corresponds to higher modes.

2. Theory of the horizontal-to-vertical spectral ratio (HVSR)

It has been established that the HVSR, defined as the square root of the ratio between the horizontal and the vertical power spectral densities in a diffuse field, can be expressed in terms of the imaginary parts of the Fourier-transformed Green functions for coinciding source and receiver (Sánchez-Sesma *et al*., 2011). In particular, this quantity can be expressed in term of the imaginary part of the Green's function components as:

$$\text{H/V}(\boldsymbol{x}, \omega) = \sqrt{\frac{\text{Im}[G_{11}(\boldsymbol{x}, \boldsymbol{x}; \omega)] + \text{Im}[G_{22}(\boldsymbol{x}, \boldsymbol{x}; \omega)]}{\text{Im}[G_{33}(\boldsymbol{x}, \boldsymbol{x}; \omega)]}}. \tag{1}$$

where $\text{Im}[G_{11}(\boldsymbol{x}, \boldsymbol{x}; \omega)]$ is the imaginary part of the Green function and $G_{11}(\boldsymbol{x}, \boldsymbol{x}; \omega)$ is the displacement at x in direction 1 produced by a unit harmonic load acting at x in direction 1. The subscript 1 and 2 refer to horizontal, and 3 to vertical degrees of freedom, and ω stands for circular

5

frequency. Eq. (1) gives the way to compute the HVSR theoretically, assuming that the wavefield can be approached by a diffuse field. In this expression, the Green function components are associated with the geometry and the elastodynamic properties of the ground. In this work, a layered halfspace with unbounded horizontal interfaces is considered. The top surface is a free surface and the media are assumed homogeneous, isotropic and elastic, with P and S wave velocities α_i and β_i, mass density ρ_i and thickness h_i for layer i. Further details about the efficient computation of HVSR are described in García-Jerez *et al.* (2016).

3.- Relationship between dispersion curves and HVSR

The theoretical relationship between the dispersion curve and the HVSR comes from the calculation of the imaginary part of the main diagonal of the Green's tensor under a diffuse field approach. These quantities can be expressed, for a given frequency, as integrals on the horizontal (radial) wavenumber k. The kernels in the (k, ω) domain can be extended to the complex k-plane. Since surface waves correspond to simple poles along the real-k axis, their contributions to the integrals can be computed from the Cauchy's residue theorem. As shown in García-Jerez *et al.* (2016), the expressions for the imaginary part of the Green's function, in the special case of source and receiver coinciding at the top of the layered media, can be written in a very compact form:

$$\text{Im}[G_{11}(0,0;\omega)] = \text{Im}[G_{22}(0,0;\omega)] =$$

$$= \underbrace{-\frac{1}{4}\left(\overbrace{\sum_m \chi_m^2 A_{Rm}}^{Rayleigh} + \overbrace{\sum_m A_{Lm}}^{Love} \right)}_{Surface\ waves} + \underbrace{\frac{1}{4\pi} \int_0^{\omega/\beta_N} Re\left[f_{PSV}^H(k) + f_{SH}(k) \right]_{4^{th}} dk}_{Body\ waves}; \tag{2}$$

$$\text{Im}[G_{33}(0,0;\omega)] = \underbrace{-\frac{1}{2}\left(\overbrace{\sum_m A_{Rm}}^{Rayleigh} \right)}_{Surface\ waves} + \underbrace{\frac{1}{2\pi} \int_0^{\omega/\beta_N} Re\left[f_{PSV}^V(k) \right]_{4^{th}} dk}_{Body\ waves};$$

where $f_{PSV}^H(k)$, $f_{PSV}^V(k)$ and $f_{SH}(k)$ are the kernels associated to the body waves in 3-D, χ_m is the

6

ellipticity of the mth Rayleigh mode, and A_{Rm} and A_{Lm} correspond to the medium responses for the mth Rayleigh and Love modes, respectively (Harkrider, 1964). The analytical computation of χ_m, A_{Rm} and A_{Lm} requires the precise location of the poles along the real k-axis. These positions can be evaluated rapidly as they correspond to the values of the $k_m(\omega)$ representation of the dispersion curves at a given frequency (see *e.g.* Piña-Flores *et al.* 2016). In summary, under the DFA, the HVSR contains implicit information on the fundamental- and higher-modes phase velocity dispersion curves.

The examination of two example models listed in Table 1 will provide insight into the relationship between the Rayleigh wave dispersion curves and the shape of the HVSR. Model 1 consists of a layer overlaying a stiffer half-space, while two layers with two significant impedance contrasts are considered for model 2. Velocity increases downwards and impedance contrasts between the layers are high enough to exemplify the osculation effect between the fundamental mode and the first higher mode. Rayleigh wave dispersion curves for model 1 are shown in figure 1 for the fundamental and the first higher mode and for both phase and group velocities, along with the theoretical HVSR computed under the DFA.

Table 1. Example models used in this work.

h (m)	α(m/s)	β(m/s)	ρ(kg/m^3)
Model 1			
25	663	200	1700
∞	866	500	2200
Model 2			
15	2000	380	1600
350	2300	850	1800
∞	3500	2000	2500

Two characteristic frequencies can be identified in the HVSR. The first frequency corresponds to the main peak (approximately coincident with the fundamental resonance frequency of the S waves) and the second one corresponds to the absolute minimum (close to the fundamental resonance frequency of the P waves, see Piña-Flores *et al.*, 2017). These two frequencies are often in the frequency band of interest for geotechnical studies, in particular, the peak frequency. Other important properties are the frequencies of the inflection points in the phase velocity dispersion curves (f_{Inf}, points where the concavity of the dispersion curve changes) and the frequencies of the critical points in the group velocity curves (f_{crit}, points where the first derivative, respect to frequency f vanishes), that is:

$$\frac{d^2c(f_{Inf})}{df^2} = 0 \text{ and } \frac{dU(f_{crit})}{df} = 0, \tag{3}$$

where $\frac{d^2c(f)}{df^2}$ is second derivative of phase velocity dispersion curve and $\frac{dU(f)}{df}$ is the first derivative of the group velocity. $\frac{d^3c(f_{Inf})}{df^3} \neq 0$ has been assumed.
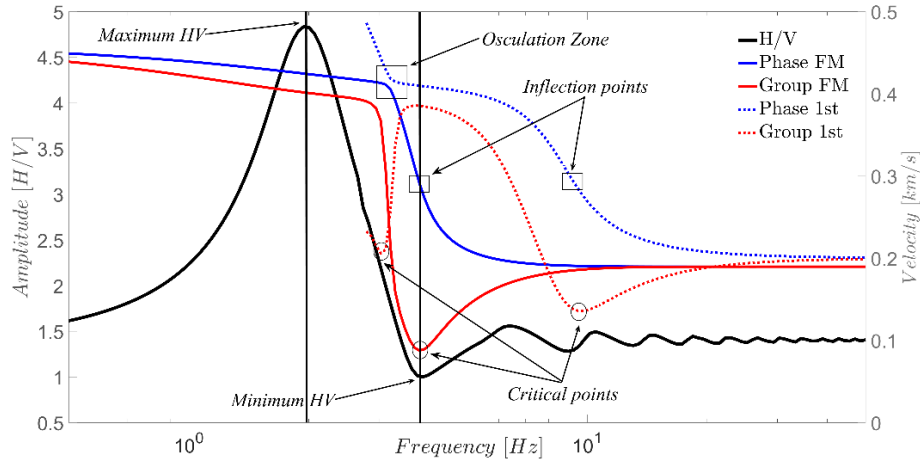

Figure 1: HVSR (continuous black line) and dispersion curves of Rayleigh waves for group velocity (red lines) and phase velocity (blue lines) computed for model 1. Small circles point to the critical points of the group velocity curves while the small squares show the inflection points of the phase velocity curves. The frequency of the inflection point and critical point, for the fundamental mode, are very close to the minimum of the HVSR. The frequencies where possible osculation effects exist are between the first maximum and the first minimum of the HVSR.

A first relationship between the inflection points of the phase velocity dispersion curves and the shape of the HVSR can be stated considering the frequency of the first minimum of the HVSR. This frequency is next to the frequency of the inflection point of the fundamental-mode dispersion curve. This same pattern can be observed for the first higher mode where the frequency of the inflection point is close to the second minimum of the HVSR. Another characteristic of the phase velocity dispersion curves is that they may have zones of osculation between modes. This osculation between the fundamental mode and the first higher mode is present between the frequencies of the main peak and the first minimum of the HVSR.

The relationship between the HVSR and the group velocity dispersion curve is also evident. The frequency of the minimum in the HVSR is close to the frequency of the critical point of the dispersion curve, even with a higher degree of proximity in comparison with the inflection point. Additionally, the frequency of the first crossing between the fundamental mode and the first higher mode in group velocity is between the main peak and the first minimum. Besides, we can observe a critical point of the group velocity curve for the higher mode in this frequency range.

Figure 2 shows the calculation of the fundamental mode and the first higher mode for phase and group velocity of Rayleigh waves for model 2, along with the HVSR. For this model, the HVSR shows two prominent peaks and two clear troughs. In the same way as the previous example, we can observe the mentioned behavior of the dispersion curves between the frequencies of the maximum and minimum for the two peak-trough pairs. That is, the frequencies where the HVSR presents these minima approximately correspond to the locations of inflection points in the phase velocity curve and of critical points in the group velocity curve, both for fundamental mode.

The effects of osculation are present between the frequencies of the maximum and minimum of the HVSR. The group velocity dispersion curves present several crossings between the higher modes and the fundamental mode at different frequencies, making it difficult to distinguish the fundamental mode. In the analyzed models, at least a crossing between the fundamental and the first higher mode of group velocity appears between the maximum and minimum of the HVSR.
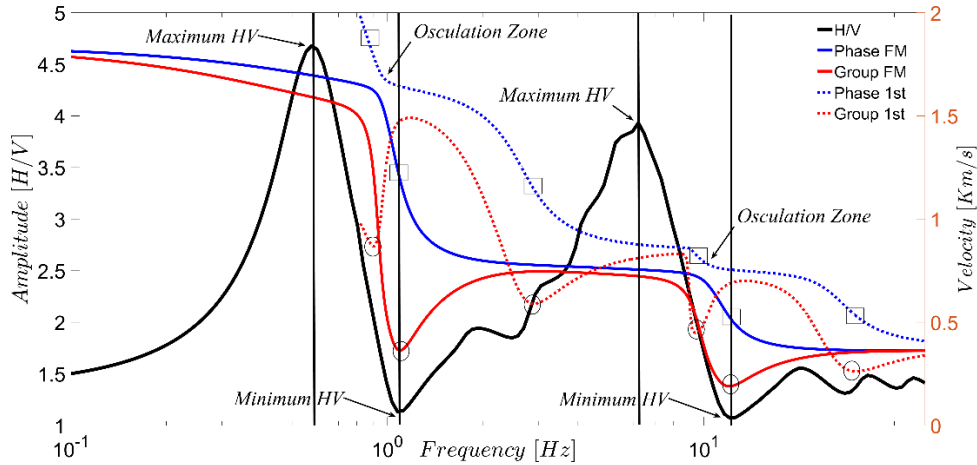
Figure 2: HVSR (black line) and dispersion curves of Rayleigh waves for group velocity (red lines) and phase velocity (blue lines) computed for model 2. The critical points of the group velocity curves are shown with circles, while the squares show the inflection points for the phase velocity curves. Frequencies of inflection points and critical points in the fundamental mode are next to the troughs of the HVSR. Possible osculation effects appear between the frequencies of the maximum and minimum of the HVSR.

Figure 3 shows the dispersion curves of the fundamental mode for phase (panel b) and group (panel c) velocity of Rayleigh waves along with the HVSR (panel a) modifying the thickness of the surface layer in model 1 (from 10 up to 110 m). Figure 3d shows the frequencies of the critical and inflection points of the dispersion curves (in group and phase velocity, respectively) and the minima in the HVSR as a function of the thickness of the top layer. Note that the variation in thickness in this high-contrast model does not modify the correspondence among the frequencies of critical, inflection points and troughs.

Following with this parametric analysis, variations in the velocity contrast of model 1 have been also considered (Figure 4). To do so, several S-wave velocities of the surface layer, β_1, have been taken from 150 to 450 m/s. The thickness has been also modified in order to keep β_1/h constant (it approximately preserves the peak frequency of the HVSR). The Poisson ratio of the layer (0.45) and the properties of the halfspace have been also kept constant. Figure 4d shows the evolution of the critical and inflection points in the dispersion curves (group and phase velocity, respectively) and of

10

the minima of HVSR as β_1 varies. Note that the approximate coincidence in frequency between the critical point in $U(f)$ and the trough in HVSR(f) persists. The frequencies of the inflection point in $c(f)$ and of the minimum in HVSR(f) exhibit better correspondence for those models with high impedance contrast producing amplitudes higher than two at the main HVSR peak.
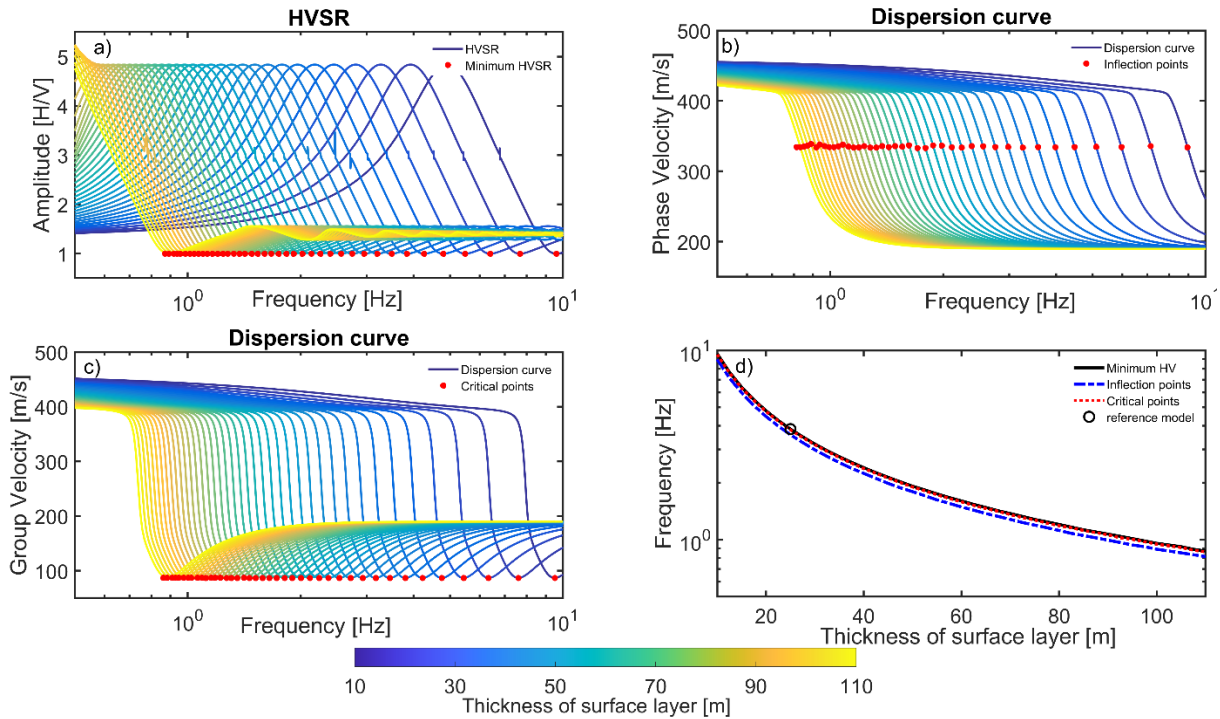

Figure 3: Fundamental-mode dispersion curve for phase (panel b) and group (panel c) velocities of Rayleigh waves, and HVSR (panel a) obtained from model 1 modifying the thickness of the surface layer (from 10 to 110 m). Red dots represent inflection and critical points of dispersion curves and minima of the HVSR. Panel d shows the frequencies of such points as a function of the layer thickness.
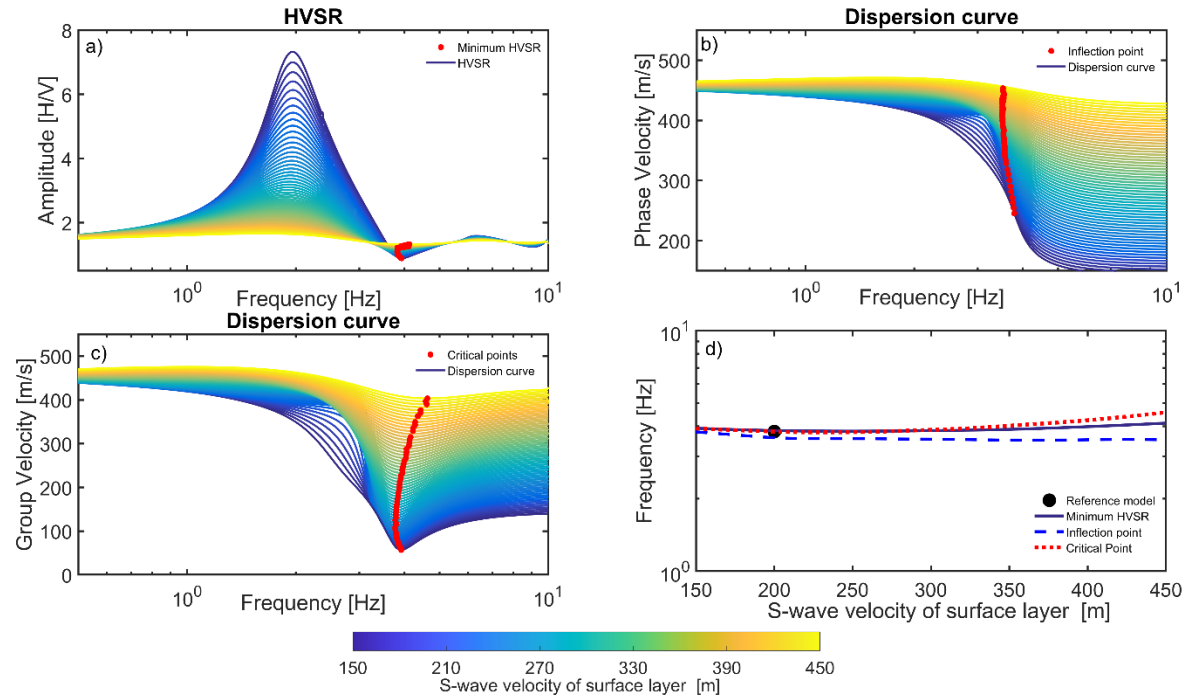
Figure 4: HVSR (panel a) and fundamental-mode dispersion curves for phase (panel b) and group (panel c) velocities of Rayleigh waves obtained from model 1 modifying the velocities and thickness of the upper layer. β_1 ranged from 150 to 450 m/s; the Poisson ratio of the layer and the β_1/h ratio are preserved. Red points represent inflection points in $c(f)$, critical points in $U(f)$ and minima in the HVSR(f). Panel d shows the variation of the frequencies of the mentioned points as β_1 varies.

4.- Application to experimental data in the Andarax river delta (Almería, Spain)

In order to obtain a representative velocity profile for the Andarax river delta, ASN data were recorded using five sensors in pentagonal array configurations with radii of 12, 25, 50, 94 and 420 m. Identification of dispersion curves for the fundamental mode of Rayleigh waves was done by using the SPAC, FK and HVSR techniques using the Geopsy software (Wathelet *et al*., 2008, Köhler *et al*., 2007, http://www.geopsy.org/, last accessed February 2017). The time windowing used for processing ranged from 40 s to 120 s long with a 50% overlapping between consecutive windows. Rayleigh-wave group-velocity dispersion diagrams were also obtained from the CC between pairs of receivers using frequency-time analysis (FTAN, e.g. Bensen *et al*., 2007). The application of the SPAC, FK and CC techniques was carried out using ~2 hours of ASN records at array "A" site (Figure 5). Since

12

wind, poor thermal isolation, etc. can generate instability in the HVSR at low frequencies, an 8 h record from a nearby permanent broadband station properly installed in the campus of the University of Almería was used to calculate the HVSR. In this way, the curve was be safely extended below 0.2 Hz to better show the shape of the main peak. For frequencies around and above the main peak, this spectral ratio does not differ significantly from those taken at the array site with portable seismometers.
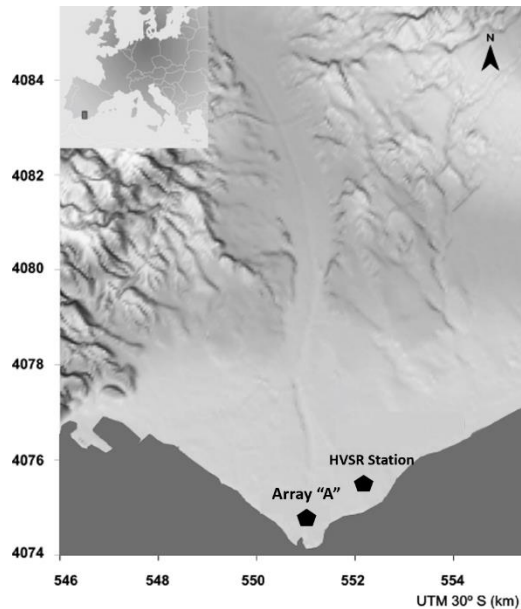

Figure 5: Location of array "A" measurements and HVSR station (UTM coordinates).

Figure 6 shows the dispersion diagrams obtained and the HVSR for the study area. From the dispersion diagram derived from the SPAC technique (figure 6a) it is possible to observe a possible discontinuity or jump from the fundamental mode to the higher mode in the range from 0.6 to 0.8 Hz. In the range between 0.8 and 2 Hz the fundamental mode dispersion curve emerges clearly. In the frequency band between 1.72 and 4 Hz the phase velocity seems to increase as the frequency increases. This type of phenomenon can occur in two cases where: 1.-the medium has a low velocity zone (LVZ); 2. - higher modes are present (Tokimatsu *et al*., 1992). For the first case, the existence of an LVZ can be ruled out because the amplitude of curve of HVSR is not less than the unit in the entire range of observation frequencies (Castelaro & Mulargia, 2006) and, consequently, we associate

this effect to higher modes. Finally, in the range from 4 to 8 Hz, the dispersion diagram shows a part of the fundamental mode dispersion curve with severe contamination by higher modes that makes picking difficult.

From another perspective, the dispersion diagram obtained from the FK technique (figure 6b) clearly shows the fundamental mode dispersion curve in the frequency range from 4 to 10 Hz (where its identification from SPAC technique was unclear). The bump in the frequency band from 1.5 to 3.8 Hz can be associated with the presence of higher modes, as in the case of the dispersion diagram derived from SPAC. In the band between 0.5 and 1 Hz, this method provided poor resolution and the trend of the dispersion curve is unclear. On the other hand, in the dispersion diagram obtained from the CC technique (figure 6c) it is possible to observe the group-velocity dispersion curve in the frequency range between 0.7 and 7 Hz. In this case, the wide range of observation frequencies for the dispersion curve may be associated to a softer transition between different modes, which may show very close group velocities. Note that higher mode group velocity curves might cross each other, and even the fundamental mode. Finally, the HVSR (figure 6d) presents two main peaks at 0.38 and 2.5 Hz and two minima at 0.79 and 5 Hz, respectively. Small oscillations that do not represent main peaks are observed in the frequency range between 0.8 and 2.5 Hz.

As mentioned in the previous section, observation of the shape of the HVSR curve is handy for identifying the fundamental mode and those bands with possible osculation and multimode effects in the dispersion diagrams, which correspond to the frequencies between and around the main maxima and minima of the HVSR. The frequencies of the troughs in the HVSR (0.8 and 5 Hz in this case) indicate the proximity of inflection points in the phase dispersion curve. As mentioned above, the dispersion diagrams derived from FK and SPAC techniques exhibit well defined velocities in the range from 2.5 to 4 Hz which corresponds to energy of higher modes. In many cases, this effect causes an erroneous identification of the dispersion curve. However, the HVSR indicates that a multimode or osculation effect is expected in the frequency range between 0.38 (first peak) and 0.8 Hz (first trough) and between 2.5 (second peak) and 5 Hz (second trough). In the dispersion diagram computed from the CC technique, two critical points are observed at 0.8 and 5 Hz, corresponding with the
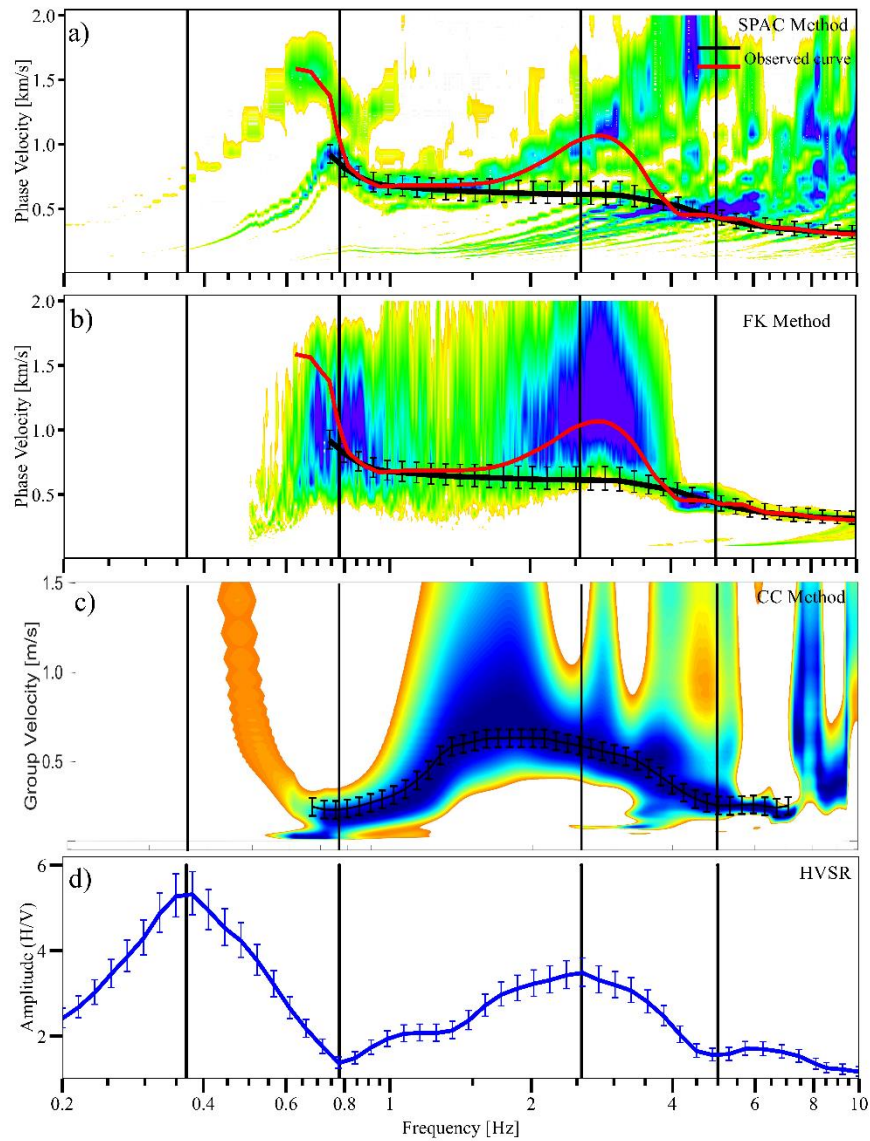
14

Figure 6: Dispersion diagrams and HVSR obtained at the Andarax river delta (figure 5). a) Dispersion diagram (phase velocity) by applying the SPAC method. b) Dispersion diagram (phase velocity) applying the FK method. c) Dispersion diagram (group velocity) applying the CC method. d) HVSR. The solid black line in the dispersion diagrams shows the fundamental mode dispersion curve, picked considering the shape of the HVSR. The solid red line in the dispersion diagrams shows a possible alternative dispersion curve, picked according to the criteria of maximum energy bands (effective curve). The vertical black lines in all the panels represent the frequencies of the relevant maxima and minima of the HVSR which can be used for identification of possible inflection points, osculation zones and multimode effects in the dispersion diagrams.

minima of the HVSR. Instead, if only the criterion of maximum energy is taken, we can obtain an effective dispersion curve from the dispersion diagrams. An example of a possible effective curve is shown in figure 6ab (solid red line), presenting an inversion of phase velocities. The inversion of that curve as the fundamental mode would lead to an unreliable model with significant intermediate low-velocity layers.

Besides, the amplitude of the peaks in the HVSR is an indicator of the impedance contrasts between the corresponding layers of the medium, and hence of the expected trend of the dispersion curves. That is, the amplitude of the peaks in the HVSR increases as the slope of the fundamental-mode phase-velocity curve increases (in absolute value). As shown in figure 6d, the main peak at high frequencies (5 Hz) has an amplitude of 3.5 while the main peak at low frequencies (0.79 Hz) exhibits an amplitude of 5.5. Therefore, we can expect a sharper variation in phase velocity around 0.79 Hz. Once the dispersion curve was picked, a joint inversion of HVSR and dispersion curve was performed using the HV-Inv free software (https://w3.ual.es/GruposInv/hv-inv/, last accessed June 2018) to obtain a representative estimation of the velocity profile of the zone. Figure 7 shows the result of the inversion which exhibits an excellent agreement between the observed HVSR, phase-velocity and group-velocity dispersion curves and the theoretical counterparts in the whole frequency range. The joint inversion of these curves allowed to estimate the velocity structure at the test site in the mouth of Andarax river, defined by α and β velocity structures and ρ structure. Piña Flores *et al.* (2017) suggested that the minimum number of layers to consider for an HVSR inversion should be equal to the number of main peaks. Since three main peaks are visible on the HVSR here, a profile with three layers on top on a half-space has been considered. Table 2 lists the parameters of the model which best fitted the observations, which shows an estimated bedrock depth of 0.43 km with β of 1810 m/s. The depth of the basement agrees well with the results of independent geophysical studies carried out in the '80 s by the Spanish Geological Survey (IGME, 1983). The theoretical dispersion curves for phase and group velocities of higher modes were calculated for the inverted model and incorporated in the experimental dispersion diagrams (see figure 8). This figure evidences that some high energy zones in dispersion diagrams correspond to higher modes.
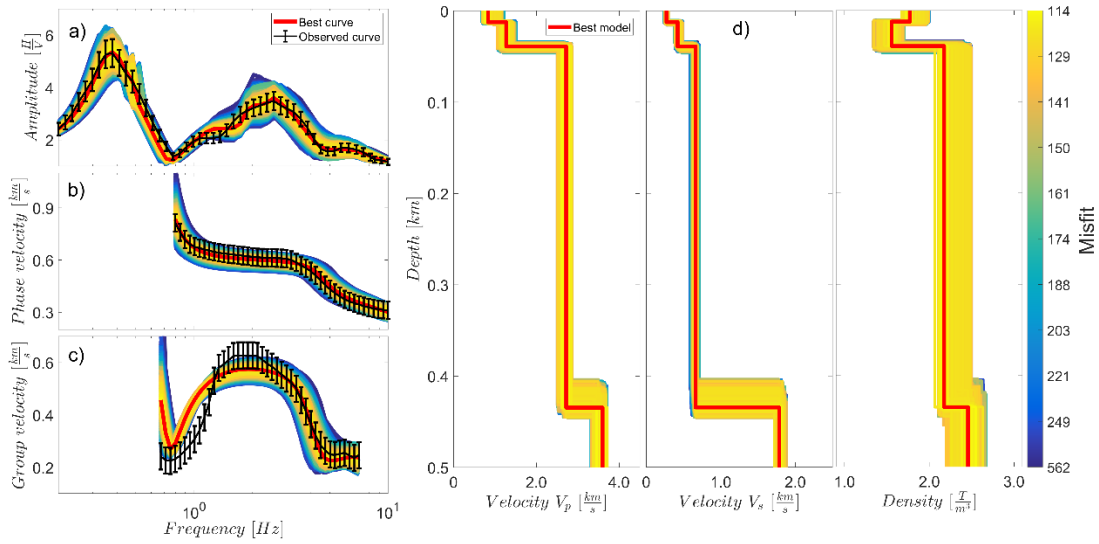
Figure 7: Results from joint inversion at the test site in the mouth of the Andarax river. a) Target HVSR (black line) and theoretical HVSR for the best-fitting model (red line). b) Experimental phase-velocity dispersion curve (black line) and theoretical dispersion curve for the best fitting model (red line). c) Experimental group velocity dispersion curve (black line) and theoretical dispersion curve for the best fitting model (red line). d) Velocity and density profiles results from simultaneous inversion. The colored curves are associated with the trial models generated by the iterative inversion method. The bedrock depth is estimated from the best fitting model at 0.43 Km and agrees well with geophysical prospecting carried out by the Spanish Geological Survey (IGME 1983).

Table 2. Best model inverted at the Andarax river test site.

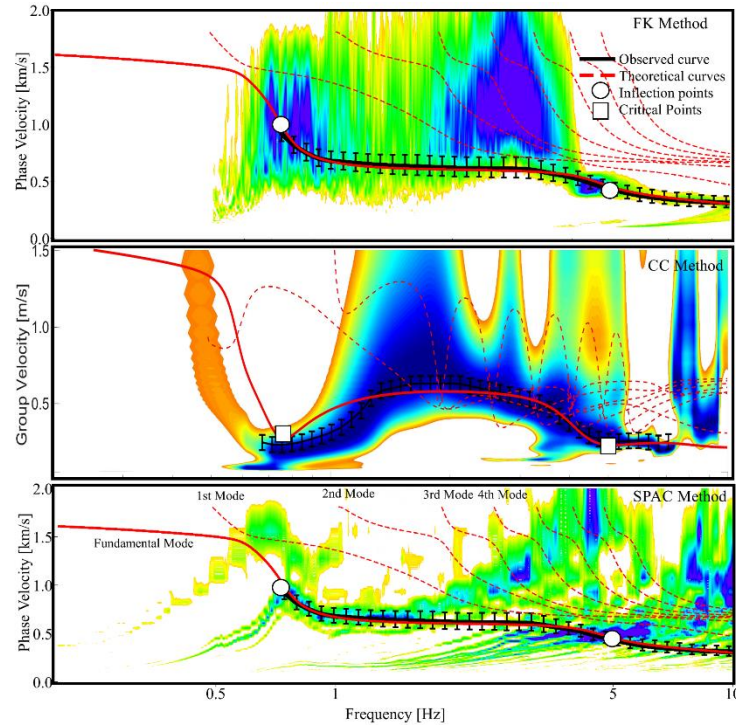| h (m)	α(m/s)	β(m/s)	ρ(kg/m^3)
Proposed velocity profile			
12	828	270	1749
26	1269	420	1538
395	2705	662	2165
∞	3538	1810	2500

17

Figure 8: Dispersion diagrams shown in figure 6, including theoretical dispersion curves of several modes (solid and dashed red lines) calculated from the velocity profile obtained from joint inversion of the observed dispersion curves and the HVSR (solid black lines). The squares point to the critical points of the fundamental-mode group-velocity dispersion curve, while the circles show the inflection points of the fundamental-mode phase-velocity dispersion curve.

3. Conclusions

In this work, we explore the relationship between the behavior of the group and phase velocity dispersion curves for the fundamental and first higher mode of Rayleigh waves and the HVSR interpreted under the diffuse field theory. The relationship between these two curves can be summarized in the following five points.

1.-The inflection and critical points in the dispersion curves can be used as control points to distinguish the fundamental mode from the higher ones. This knowledge is of great help for the correct picking of phase and group Rayleigh-wave modes from the dispersion diagrams.

2. For the fundamental mode, the frequencies of the inflection points in the phase-velocity dispersion

curve and of the critical points in the group-velocity curve are very close to the frequencies of the main troughs of the HVSR.

3. The osculation effect between the fundamental mode and the first higher mode is located between the frequencies of the main peaks and the following minima of the HVSR.

4.-The band with possible effect of multiple modes is located between the frequencies of the main peak and the subsequent minimum of the HVSR.

5. The amplitude of the main peaks of the HVSR increases as the slope (in absolute value) of the phase-velocity dispersion curve increases.

As an example, we used the HVSR to assist in the identification of fundamental mode phase and group velocity dispersion curves from dispersion diagrams in the Andarax river delta (SE Spain). A reliable velocity profile for the zone was obtained from joint inversion of these three curves. We propose to use information in the HVSR of ASN to identify the osculation zones, multi-mode effect, inflection points and critical points of the fundamental mode from the dispersion diagrams. This way of proceeding can be a very useful complementary tool along with other ways of mode identification. It allowed to obtain a representative velocity profile of the zone using joint inversion, aimed at obtaining a more accurate assessment of local site effects in the event of an earthquake.

Acknowledgements

References

Aki, K., 1957. Space and time spectra of stationary stochastic waves, with special reference to microtremors. *Bulletin of the Earthquake Research Institute*, University of Tokyo **35**, 415–457.

Arai, H. & Tokimatsu, K., 2004. S-wave velocity profiling by inversion of microtremor H/V spectrum, *Bull. Seism. Soc. Am.,* **94**(1), 53–63.

Astaneh, A. V. & Guddati, M. N., 2016. Improved inversion algorithms for near-surface characterization. *Geophys. J. Int.* **206**, 1410–1423 doi: 10.1093/gji/ggw192.

Baena-Rivera, M., Perton, M. & Sánchez-Sesma, F. J., 2016. Surface-Wave Retrieval from Generalized Diffuse Fields in 2D Synthetic Models of Alluvial Valleys. *Bull. Seism. Soc. Am.,* Vol. **106**, No. 6, pp. doi: 10.1785/0120160084

Bensen, G.D., Ritzwoller, M. H., Barmin, M. P., Levshin, A. L. Lin, F., Moschetti, M. P., Shapiro N. M. and Yang, Y., 2007. Processing seismic ambient noise data to obtain reliable broad-band surface wave dispersion measurements. *Geophys. J. Int.* **169**, 1239–1260 doi: 10.1111/j.1365-246X.2007.03374.x.

Boaga, J., G. Cassiani, C. L. Strobbia, and G. Vignoli., 2013, Mode misidentification in Rayleigh waves: Ellipticity as a cause and a cure: *Geophysics*, **78**, no. 4, EN17–EN28, doi: 10.1190/geo2012-0194.1.

Bonnefoy-Claudet, S., Cotton, F., & Bard, Pierre-Yves., 2006. The nature of noise wavefield and its applications for site effects studies: A literature review. *Earth-Science Reviews* **79** 205–227**.** doi:10.1016/j.earscirev.2006.07.004

Boué, P., Denolle, M., Hirata, N., Nakagawa, S., & Beroza, G. C., 2016. Beyond basin resonance: characterizing wave propagation using a dense array and the ambient seismic field. *Geophys. J. Int.* **206**, 1261–1272. doi: 10.1093/gji/ggw205

Capon, J., 1969. High-resolution frequency-wavenumber spectrum analysis, *Geophysics.* **34,** no. 1, 21–38.

Castelaro, S. & Mulargia, F., 2006. The Effect of Velocity Inversions on H/V, *Pure Appl. Geophys.* **166**, 567–592. doi: 10.1007/s00024-009-0474-5

Coelho, M. J., Santos, J., & Pereira, M., 2018. Stacking of multilayout and multichannel surface-wave data on the f-k domain. *J. Appl. Geophys.*, **159**, 93-107. doi: 10.1016/j.jappgeo.2018.08.006

Dai, K., Liu, K., Li, X., You, Q., Tang, H., & Xu, Q., 2019. Application of passive multichannel analysis of surface waves method at sites close to underground railways-Problems and a case study. *J. Appl. Geophys.*, 164, 191-199. doi: 10.1016/j.jappgeo.2019.03.009

Farrugia, D., Paolucci, E., D'Amico, S., & Galea, P., 2016. Inversion of surface wave data for subsurface shear wave velocity profiles characterized by a thick buried low-velocity layer. *Geophys. J. Int.*, **206**(2), 1221-1231. doi: 10.1093/gji/ggw204

Foti, S., Parolai, S., Albarello, D. & Picozzi, M., 2011. Application of Surface-Wave Methods for Seismic Site Characterization. *Surveys in Geophysics*, **32**(6), 777-825. doi: 10.1007/s10712-011-9134-2.

Gao, L., Xia, J., & Pan, Y., 2014. Misidentification caused by leaky surface wave in high-frequency surface wave method. *Geophys. J. Int.*, **199**(3), 1452-1462. doi: 10.1093/gji/ggu337

Gao, L., Xia, J., Pan, Y., & Xu, Y., 2016. Reason and Condition for Mode Kissing in MASW Method. *Pure Appl. Geophys*, **173**(5), 1627-1638. doi: 10.1007/s00024-015-1208-5

García-Jerez A., F. J. Sánchez-Sesma., 2015. Slowly-attenuating P-SV Leaky Waves in a Layered Elastic Halfspace. Effects on the Coherences of Diffuse Wavefields. *Wave Motion*, **54**, 43–57. doi: i.org/10.1016/j.wavemoti.2014.11.010

García-Jerez, A., Luzón, F., Navarro, M. & Pérez-Ruiz, J. A., 2008. Determination of elastic properties of shallow sedimentary deposits applying a spatial autocorrelation method. *Geomorphology.* **93,** 74–88. doi: 10.1016/j.geomorph.2006.12.018

García-Jerez, A., Piña-Flores, J., Sánchez-Sesma, F. J., Luzón, F., & Perton, M., 2016. A computer code for forward computation and inversion of the H/V spectral ratio under the diffuse field assumption, *Comput. Geosci.*, **97**, 67–78. doi: 10.1016/j.cageo.2016.06.016

García-Jerez, A., Seivane, H., Navarro, M., Martínez-Segura, M., & Piña-Flores, J., 2019. Joint analysis of Rayleigh-wave dispersion curves and diffuse-field HVSR for site characterization: The case of El Ejido town (SE Spain). *Soil Dyn. Earthq. Eng.*, 121, 102-120. doi: 10.1016/j.soildyn.2019.02.023

Harkrider, D.G., 1964. Surface waves in multilayered elastic media I. Rayleigh and Love waves from buried sources in a multilayered elastic half-space, *Bull. seism. Soc. Am.*, **54**(2), 627–679.

IGME., 1983. Prospección geotérmica en la depresión de Almería, Vol. V,Madrid, Spain, In Spanish. Available at: http://info.igme.es/ConsultaSID/presentacion.asp?Id=800, last accessed 12 January 2020.

Ikeda, T., Matsuoka, T., Tsuji, T. & Hayashi, K., 2012. Multimode inversion with amplitude response of surface waves in the spatial autocorrelation method. *Geophys. J. Int.* **190,** 541–552 doi: 10.1111/j.1365-246X.2012.05496.x

Kawase, H., Sánchez-Sesma, F.J. & Matsushima, S., 2011. The optimal use of horizontal-to-vertical spectral ratios of earthquake motions for velocity inversions based on diffuse-field theory for plane waves, *Bull. Seism. Soc. Am.*, **101**(5), 2001–2014. doi: 10.1785/0120100263

Köhler, A., Ohrnberger, M., Scherbaum, F., Wathelet, M. & Cornou, C., 2007. Assessing the reliability of the modified three-component spatial autocorrelation technique. *Geophys. J. Int.* **168**, 779–796 doi: 10.1111/j.1365-246X.2006.03253.x.

Lai, C. G., Mangriotis, M-D. & Rix G. J., 2014. An explicit relation for the apparent phase velocity of Rayleigh waves in a vertically heterogeneous elastic half-space. *Geophys. J. Int.* **199**, 673–687 doi: 10.1093/gji/ggu283.

Lermo, J. & Chávez-García, F.J., 1993. Site effect evaluation using spectral ratios with only one station, *Bull. Seism. Soc. Am.*, **83**(5), 1574–1594.

Lin, C. P., Lin, C. H., & Chien, C. J., 2017. Dispersion analysis of surface wave testing–SASW vs. MASW. *J. Appl. Geophys.*, **143**, 223-230. doi: /10.1016/j.jappgeo.2017.05.0080926-9851.

22

Lontsi, A. M., Sánchez-Sesma, F. J., Molina-Villegas, J. C., Ohrnberger, M., & Krüger, F., 2015. Full microtremor H/V (*z*, *f*) inversion for shallow subsurface Characterization. *Geophys. J. Int.* **202**, 298–312 doi: 10.1093/gji/ggv132.

Louie, J.N., 2001. Faster, Better Shear wave velocity to 100m depth from ReMi arrays. *Bull. Seism. Soc. Am.,* **91**:2, 347-364**.**

Lunedei, E. & Albarello, D., 2009. On the seismic noise wavefield in a weakly dissipative layered Earth. *Geophys. J. Int.* **177**, 1001–1014 doi: 10.1111/j.1365-246X.2008.04062.x.

Ma, Y., Clayton, R. W. & Li, D., 2016. Higher-mode ambient-noise Rayleigh waves in sedimentary basins. *Geophys. J. Int.* 206, 1634–1644 doi: 10.1093/gji/ggw235.

Maranò, S., Hobiger, M., & Fäh, D., 2017. Retrieval of Rayleigh wave ellipticity from ambient vibration recordings. *Geophys. J. Int.* **209**, 334–352 doi: 10.1093/gji/ggx014

Maraschini, M., Ernst, F., Foti, S., & Socco, L. V., 2010. A new misfit functions for multimodal inversion of surface waves. *Geophysics*, **75**(4), G31-G43. doi 10.1190/1.3436539

Mi, B., Xia, J., Shen, C., Wang, L., Hu, Y., & Cheng, F., 2017. Horizontal resolution of multichannel analysis of surface waves. *Geophysics*, **82**(3), EN51-EN66. doi. 10.1190/geo2016-0202.1

Mi, B., Xia, J., Shen, C. and Wang, L., 2018. Dispersion Energy Analysis of Rayleigh and Love Waves in the Presence of Low-Velocity Layers in Near-Surface Seismic Surveys. *Surveys in Geophysics*. **39**, 271–288 (2018). https://doi.org/10.1007/s10712-017-9440-4

Mi, B., Hu, Y., Xia, J. and Socco, L. V., 2019. Estimation of horizontal to vertical spectral ratios (HVSR, ellipticity) of Rayleigh waves from multi-station active-seismic records, *Geophysics,* 84(6), EN81-EN92. doi: 10.1190/geo2018-0651.1

Nakamura, Y., 1989. A method for dynamic characteristics estimation of subsurface using microtremor on ground surface, *QR of RTRI*, **30**(1), 25–33.

Ning, L., Dai, T., Wang, L., Yuan, S., & Pang, J., 2018. Numerical investigation of Rayleigh-wave propagation on canyon topography using finite-difference method. *J. Appl. Geophys.*, **159**, 350-361. doi: 10.1016/j.jappgeo.2018.09.0070926-9851

Ohori, M., Mobata, A. & Wakamatsu, K., 2002. A comparison of ESAC and FK methods of estimating phase velocity using arbitrarily shaped microtremor arrays, *Bull. Seism. Soc. Am.,* **92**(6), 2323– **2332.**

Pan, Y., Xia, J., Gao, L., Shen, C., & Zeng, C., 2013. Calculation of Rayleigh-wave phase velocities due to models with a high-velocity surface layer. *J. Appl. Geophys.*, **96**, 1-6. doi:10.1016/j.jappgeo.2013.06.005

Piña-Flores, J., Perton, M., García-Jerez, A., Carmona, E., Luzón, F., Molina-Villegas, J. C., & Sánchez-Sesma, F. J., 2017. The inversion of spectral ratio H/V in a layered system using the diffuse field assumption (DFA). *Geophys. J. Int.* **208**, 577–588 doi: 10.1093/gji/ggw416.

Rivet, D., Campillo, M., Sanchez-Sesma, F., Shapiro, N. M., & Singh, S. K., 2015. Identification of surface wave higher modes using a methodology based on seismic noise and coda waves. *Geophys. J. Int*., **203**, 856–868. doi: 10.1093/gji/ggv339.

Sánchez-Sesma, F.J., Rodríguez, M., Iturrarán-Viveros, U., Luzón, F., Campillo, M., Margerin, L., García-Jerez, A., Suarez, M., Santoyo, M.A., Rodríguez-Castellanos, A., 2011. A theory for microtremor H/V spectral ratio: application for a layered medium, *Geophys. J. Int.*, **186**(1), 221–225. doi: 10.1111/j.1365-246X.2011.05064.x

Sivaram, K., Gupta, S., Kumar, S., & Prasad, B. N. V., 2018. Shear velocity structural characterization around the Lonar crater using joint inversion of ambient noise HVSR and Rayleigh wave dispersion. *J. Appl. Geophys.*, **159**, 773-784. doi: 10.1016/j.jappgeo.2019.06.0220926-9851

Spica, Z., Caudron, C., Perton, M., Lecocq, T., Camelbeeck, T., Legrand, D., Piña-Flores, J., Iglesias, A., Syahbana, D.K., 2015. Velocity models and site effects at Kawah Ijen volcano and Ijen caldera

(Indonesia) determined from ambient noise cross-correlations and directional energy density spectral ratios, *J. Volc. Geotherm. Res.*, **302**, 173–189. doi: 10.1016/j.jvolgeores.2015.06.016

Tokimatsu, K., Tamura, S. & Kojima, H., 1992. Effects of multiple modes on Rayleigh wave dispersion characteristics. *J. Geotech. Engrg.*, **118**(10): 1529-1543.

Wathelet, M., D. Jongmans, M. Ohrnberger, and S. Bonnefoy-Claudet., 2008. Array performances for ambient vibrations on a shallow structure and consequences over Vs inversion. *Journal of Seismology*, **12**, 1-19. Doi: 10.1007/s10950-007-9067-x

Xia, J., Miller, R.D. & Park C.B., 1999. Estimation of near-surface shear-wave velocity by inversion of Rayleigh waves. *Geophysics*. **64**, 3; 691-700. doi: 10.1190/1.1444578

Zeng, C., Xia, J., Miller, R. D., Tsoflias, G. P., & Wang, Z., 2012. Numerical investigation of MASW applications in presence of surface topography. *J. Appl. Geophys.*, **84**, 52-60. doi:10.1016/j.jappgeo.2012.06.004

Zhang, S. X. & Chan, L. S., 2009. Possible effects of misidentified mode number on Rayleigh wave inversion. *J. Appl. Geophys.,* **53**, 17– 29. doi: 10.1016/S0926-9851(03)00014-4

Zhang, S., 2011. Effective Dispersion Curve and Pseudo Multimode Dispersion Curves for Rayleigh Wave. *Journal of Earth Science*, Vol. **22**, No. 2, p. 226–230. doi: 10.1007/s12583-011-0175-8